# Functionalized bay-substituted perylene diimide additives for inverted organic photovoltaic devices based on P3HT/PCBM

H. DİNÇALP[a,*], O. ÇİMEN[a], G. MURAT SALTAN[a], S. İÇLİ[b]
[a] *Department of Chemistry, Faculty of Arts and Science, Celal Bayar University, Muradiye Campus, 45140 Yunus Emre-Manisa/Turkey*
[b] *Solar Energy Institute, Ege University, Bornova, 35100 Izmir/Turkey*

The photovoltaic performances of inverted organic solar cells including P3HT:PCBM active layer with perylene diimides (PDIs) substituted with different subunits at bay positions of perylene ring were investigated. The improvement of photoluminescence intensity for P3HT:PCBM blend was achieved by the increase of **PDI1** additive amount from 6.6 to 10 wt%. In P3HT:PDI1:PCBM ternary blend, preliminary results obtained from cell measurements indicated that **PDI1** dopant has improved the cell efficiency by 38% compared to the control cell. Carrier mobility studies revealed that electron or hole mobility capacities of the perylene additives in ternary blends gave a more detailed explanation for efficiencies both binary and ternary systems.

(Received December 6, 2013; accepted May 7, 2015)

*Keywords:* Perylene diimide; Organic photovoltaic; Solution processable; Inverted structure; Space charge limited current regime

## 1. Introduction

Organic solar cells using the well-known active layer which consists of the different combinations of poly(3-hexylthiophene) (P3HT) and [6,6]-phenyl $C_{61}$-butyric acid methyl ester (PCBM) have continued to tremendous attention in power conversion efficiencies (PCEs) for conversion of light into the electricity. Ternary blend films, in which additive component behaves as the sensitive material and P3HT as the charge transporting part, are promising choices to extend the spectral response of solar cell to near-infrared light region and to enhance the charge transportation. Different additive materials are used to improve PCE value such as benzothiadiazole polymer [1, 2], phenylenevinylene polymer [3], phthalocyanine small molecule [4], thiophene-ethylene oxide diblock copolymer [5], diketopyrrolopyrrole small molecule [6], new $C_{60}$ derivatives [7], bathocuproine molecule [8], PbSSe nanocrystals [9] and CdSe nanoparticles [10].

Recent studies have shown that the use of perylene/PDI additives act a serious role in collecting solar light and generating the current. Soo Han and co-workers have used a small molecule PDI in bulk-heterojunction (BHJ) devices, resulting in about a 70% increase in PCE due to an effective combination in the interfaces between P3HT and PCBM domains, when compared to a pristine P3HT:PCBM device [11]. The more increase in PCE of about 98% was accomplished by the addition of 1 wt% another type of PDI dye into the P3HT:PCBM blend [12]. When Wang et al. have doped unsubstituted perylene into P3HT:PCBM blend, they have obtained a little improvement of about 27% in PCE as compared to the P3HT:PCBM blend [13]. Also, Schmidt-Mende et al. have used a PDI dopant to increase light harvesting efficiency in BHJ solar cells. They have prepared bi-layered solar cells using hexa-*peri*-hexabenzocoronene as the charge transporting matrix and PDI as the additive component and obtained an overall increase of about 60% in PCE [14]. Erten-Ela et al. have fabricated inverted BHJ solar cells using P3HT and some aromatic diimide structures. They reported a current density of 0.72 mA/cm$^2$ exhibited from P3HT:PDI (dehydroabietyl derivative) with the 1:3 blend ratio based inverted device [15]. Also, they reported that P3HT:$C_{60}$:naphthalene diimide derivatives type inverted BHJ solar cells gave PCE values between 0.50 and 0.74% [16].

Although PDI dyes are good choices for photovoltaic applications because of their extraordinary properties, which include their high molar absorptivities in solar region [17], high electron mobilities [18], good photo-stabilities under solar irradiation [19], large optical absorptivities from visible to near-infrared spectral region [20] and high fluorescence quantum yields [21], they have generally given poor PCE values in blended with P3HT as electron donor in BHJ solar cells [22-24]. It seems that the tendency of PDI to aggregate may results in self-trapping of excitons between the layer of P3HT and PDI resulting poor PCE values in devices [20]. For this reason, the aggregation of PDI should be inhibited by adjusting the mixing ratio of the ingredients in the device structure to overcome the best morphology.

Another strategy to decrease the aggregation in PDI dyes is the attachment of different functional groups into bay positions of the perylene ring. These subunits distort the planarity of the perylene $\pi$-conjugates by rotating out

of the plane. In this regard, we have paid our attention to a series of 1,7-substituted PDI dyes (one of the studied dyes, **PDI2**, is novel) as doping material in inverted BHJ solar cells comprising of P3HT:$PC_{71}BM$ blend system. We have fabricated the photovoltaic devices by adding PDI derivatives with different blending ratios in a configuration of ITO/AZO(HT)/P3HT:PDI:$PC_{71}BM$/PEDOT:PSS/Ag(100nm). Their absorption, photoluminescence and EQE measurements have been compared with those of devices without PDI additive.

## 2. Experimental section

### 2.1 General procedures

$^{1}H$ NMR and $^{13}C$ NMR spectra were recorded on a Bruker 400 MHz spectrometer using deuterated chloroform. FT-IR spectra were recorded on a Perkin Elmer-Spectrum BX spectrophotometer preparing KBr pellets. Absorption spectra of samples were obtained using a UV–vis–NIR spectrometer (Perkin Elmer Lambda 950) in solutions and on thin films in the wavelength range of 250-900 nm. PL spectra were recorded with a Hitachi's F-7000 FL Spectrophotometer. Fluorescence and life time measurements were performed on a FLSP 920 Edinburg fluorescence phosphorescence spectrophotometer. The fluorescence decay times were determined by the single photon timing method using a laser which has been used to excite the samples at 472 nm. The Edinburgh Instruments F900 exponential reconvolution software method based on the Marquardt Levenberg algorithm [25] was utilized for calculations. Single photon timing method was used to obtain the fluorescence decay histograms in 10000 data channels. The fitted decay curve was judged by the fitting parameters such as $\chi^2$<1.2 goodness of fit. The instrument response function (IRF) was measured using a ludox scattering solution.

The redox properties of **PDI2** dye were determined cyclic voltammetry (CH instruments-Electrochemical Workstation) with a standard three-electrode electrochemical compartment. The electrolyte solution employed was 100 mM [TBA][PF6] solution in Me-CN in room temperature under nitrogen purge. Ag/AgCl, glassy carbon and Pt wire electrodes were used as reference, working and counter electrodes, respectively. The scan rate was at 50 mV/s. Ferrocene-ferrocenium ($Fe/Fe^{+}$) couple exhibiting a potential at about +0.55 V was used as internal reference for the calculation of the onset values of $E_{red}$. HOMO and LUMO energy levels of **PDI2** dye were determined by the formulas:

$E_{LUMO} = -(4.8 + E_{red}^{onset})$, $E_{red}^{onset} = E_{red}^{0} - E_{ox(ferrocene)}^{0}$, $E_{HOMO} = E_{LUMO} - E_{gap}$ [26].

### 2.2 Device preparation and testing

Active layer consisting of P3HT, $PC_{71}BM$ and PDI dyes were dissolved at concentrations of 2 wt% from *o*-dichlorobenzene (oDCB) solution. Indium tin oxide (ITO)-coated glass was cleaned by the conventional cleaning method before use. Photovoltaic devices were fabricated by doctor-blading technique. Aluminium-doped zinc oxide (AZO) was employed for inverted devices. The synthetic route and characterization of AZO precursor with its applications were outlined in the literature [27-30]. It was bladed with 40 mm/s blading rate at 40 °C, then annealed at 260 °C for 10 min under air atmosphere. Active layers having different mixing ratios were coated on top of AZO layer at a blade rate constant of 20 mm/s at 65 °C. Then, PEDOT:PSS was coated at substrate temperature of 60 °C and a blading rate of 15 mm/s, then annealed at 140 °C for 5 min in glove box, followed by evaporation with silver electrode of 100 nm.

For non-inverted solar cells PEDOT:PSS solution was deposited on ITO substrates. After annealing for 15 min at 140 °C the samples were coated with active layer consisting of PDI:$PC_{71}BM$ in 1:3 wt% ratios. Annelation of the substrates was performed at a substrate temperature of 65 °C for 10 min under air. Finally, a calcium/silver top electrode of 15/80 nm thickness was evaporated.

I-V spectra were recorded using an automated computer program controlling a Keithley 2400 SMU sourcemeter. Solar cells were illuminated under AM1.5G irradiation on an OrielSol 1A Xenon solar simulator (100 mW $cm^{-2}$). The surface of the thin films was pictured by Ambios Qscope 250 Model Atomic Force Microscope. Thicknesses of the active layers of the thin films were measured by Ambios Q1 Profilometry instrument. The EQE was detected with a lock-in amplifier (SR830, Stanford Research Systems) with current preamplifier (HMS-74) under monochromatic illumination, which was calibrated with a mono-crystalline silicon diode.

Dark I-V characterictics were measured and analysed in the space charge limited current (SCLC) regime. Hole and electron only devices are configurated with the structures ITO/PEDOT:PSS/Active Layer/PEDOT:PSS/Ag(100 nm) and ITO/AZO(HT)/Active Layer/Ca(15 nm)/Ag(80 nm), respectively. These devices were prepared by the same way as organic solar cell production. We have estimated the electron and hole mobilities according to the equation [31]:

$$J_{SCL} = \frac{9}{8}\varepsilon_0\varepsilon_r\mu\frac{V_{in}^{n}}{L^3}exp\left(\frac{0.89\times\beta}{\sqrt{L}}\sqrt{V}\right)$$

where J is the current density, V is applied voltage, $\varepsilon_r$ (2.7 for blends) and $\varepsilon_0$ are the relative dielectric constants of the organic layer and permittivity of free space ($8.85 \times 10^{-12}$ A·s/V·m), respectively, $\mu$ is the electron mobility and L (100 nm) is the thickness of the organic layer.

### 2.3 Materials

**PDI1** [32] and **PDI3** [33] were synthesized according to the well-known procedure as shown in Fig. 1. In the synthesis of compound **PDI2**, 1,7-Dibromo-perylene-3,4,9,10-tetracarboxylic dianhydride and N,N′-bis(2,6-diisopropylphenyl)-1,7-dibromoperylene-3,4,9,10-

tetracarboxylic diimide were synthesized according to the literature data [32]. All the reagents and solvents were purchased from Sigma Adrich. PEDOT:PSS was obtained from Baytron PH H.C. Starck and P3HT was supplied from Rieke Inc. for the device preparation.

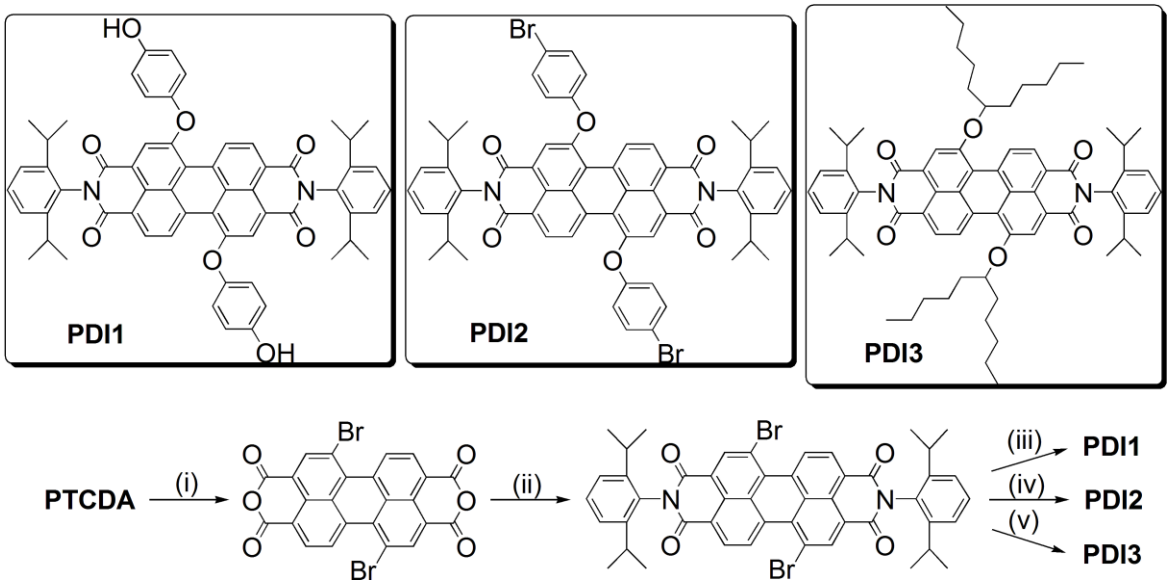


*Fig. 1. Synthesis and chemical structures of the main organic compounds used in this study. (i) $H_2SO_4$/Oleum, $Br_2$, 85 °C, 84%; (ii) 2,6-Diisopropylaniline, propionic acid, 130 °C, 72%; (iii) Hydroquinone, DMF, $K_2CO_3$, 150 °C, 60%; (iv) 6-Undecanol, DMF, $K_2CO_3$, 80 °C, 50%; (v) 4-Bromophenol, DMF, $K_2CO_3$, 150 °C, 58%.*

### 2.4 Synthesis

#### 2.4.1 Synthesis of N,N′-bis(2,6-diisopropylphenyl)-1,7-bis(4-bromophenoxy)perylene-3,4,9,10-tetracarboxylic diimide (PDI2)

N,N′-bis(2,6-diisopropylphenyl)-1,7-dibromoperylene-3,4,9,10-tetracarboxylic diimide (0.17 g, 0.20 mmol), 4-bromophenol (0.28 g, 1.63 mmol) and dry $K_2CO_3$ (0.3 g, 2.17 mmol) were suspended in dry DMF (15 mL). The mixture was stirred for 2 h at 150 °C. After cooling to room temperature, $H_2O$ (15 mL) was added, the reaction mixture was filtered and washed thoroughly with $H_2O$ (50 mL). The filter cake was dried and washed out with methanol/water solution to extract the crude product. Chromatography on silica using *n*-hexane:ethyl acetate:acetic acid (41:8:1) afforded a purple solid. Yield 58%, FT-IR (KBr $cm^{-1}$): 2925 (aliphatic $\nu_{C-H}$), 1704 ($\nu_{C=O}$), 1667 ($\nu_{C=O}$), 1591 (aromatic $\nu_{C=C}$), 1482, 1414, 1339 ($\nu_{C-N}$), 1266 ($\nu_{C-O}$), 1203, 839, 739 $cm^{-1}$. $^1$H NMR (400 MHz, $CDCl_3$, $\delta$ 7.26 ppm): $\delta$ = 9.64 (2H, d, $J$ = 7.8 Hz), 8.77 (2H, m), 8.41 (2H, s), 7.57 (2H, t, $J$ = 7.8 Hz), 7.51 (4H, m), 7.37 (6H, m), 7.01 (2H, d, $J$ = 9.0 Hz), 2.78 (4H, septet, $J$ = 7.0 Hz), 1.18 (24H, d, $J$ = 7.0 Hz ppm. $^{13}$C NMR (100 MHz, $CDCl_3$, $\delta$ 77.5 ppm, 3 peaks): $\delta$ = 164.7 (C=O), 163.9 (C=O), 156.2, 154.7, 153.9, 145.8, 133.6, 132.5, 131.4, 130.6, 130.1, 129.9, 126.6, 124.3, 122.3, 121.5, 120.5, 117.4, 29.9, 24.3 ppm.

## 3. Results and discussion

### 3.1 Optical and CV measurements

The normalized absorption spectra of **PDI1-3** dyes on thin films are shown in Fig. 2a. All series of dye show characteristic PDI absorption band around 570 nm indicating the $S_0$-$S_1$ transition state with a small shoulder band at 527 nm, excluding **PDI1** dye. The absorption spectrum of **PDI1** dye gives a small bathochromic shift of 8 nm and displays a broad band on thin film measurement compared to the corresponding spectra for other dyes. Intramolecular hydrogen bonding among the hydroxyl groups of **PDI2** dye facilitates the aggregate formation which is the major cause the change of the absorption band. Other bands around 400 nm attributes to the $\pi$–$\pi$* transition of benzene rings. In more polar Bz-CN solution (Fig. 2b), novel **PDI2** dye has strong absorption bands around 400-500 and 600-900 nm indicating the intramolecular exciplex formation of PDI dye as reported previously in the literature [32-37]. Also, Fig. S1 illustrates **PDI2** absorption covering the whole solar spectra and supports the photoinduced electron transfer process in ethanol solution. When **PDI2** dye is excited at 485 nm, where the perylene core absorbs strongly, standart emission signal around 580 nm with a shoulder at 630 nm is observed in both polar solution. Single-photon analysis of **PDI2** dye gives a three-exponential decay in Bz-Cl, Bz-CN and ethanol solutions as given in Table 1 and illustrated in Fig. 2c (for Bz-Cl). The highest decay values for all compounds may be attributed to the stationary

fluorescence of PDI core. Fast decay components below 1 ns can be attributed to the photoinduced energy transfer process between the different conformers of **PDI2** dye giving small rotations around the perylene core when excited at 485 nm. Poor fluorescence quantum yields for **PDI2** dye (0.19 for ethanol, 0.05 for Bz-CN) indicate the low abundance of PDI stationary emission at the excitation wavelength of 485 nm. This observation may be attributed to the generation of new species from the excited state of PDI structure. Detailed photophysical analysis of other studied dyes, **PDI1** and **PDI3**, are given in our previous studies [32, 33].

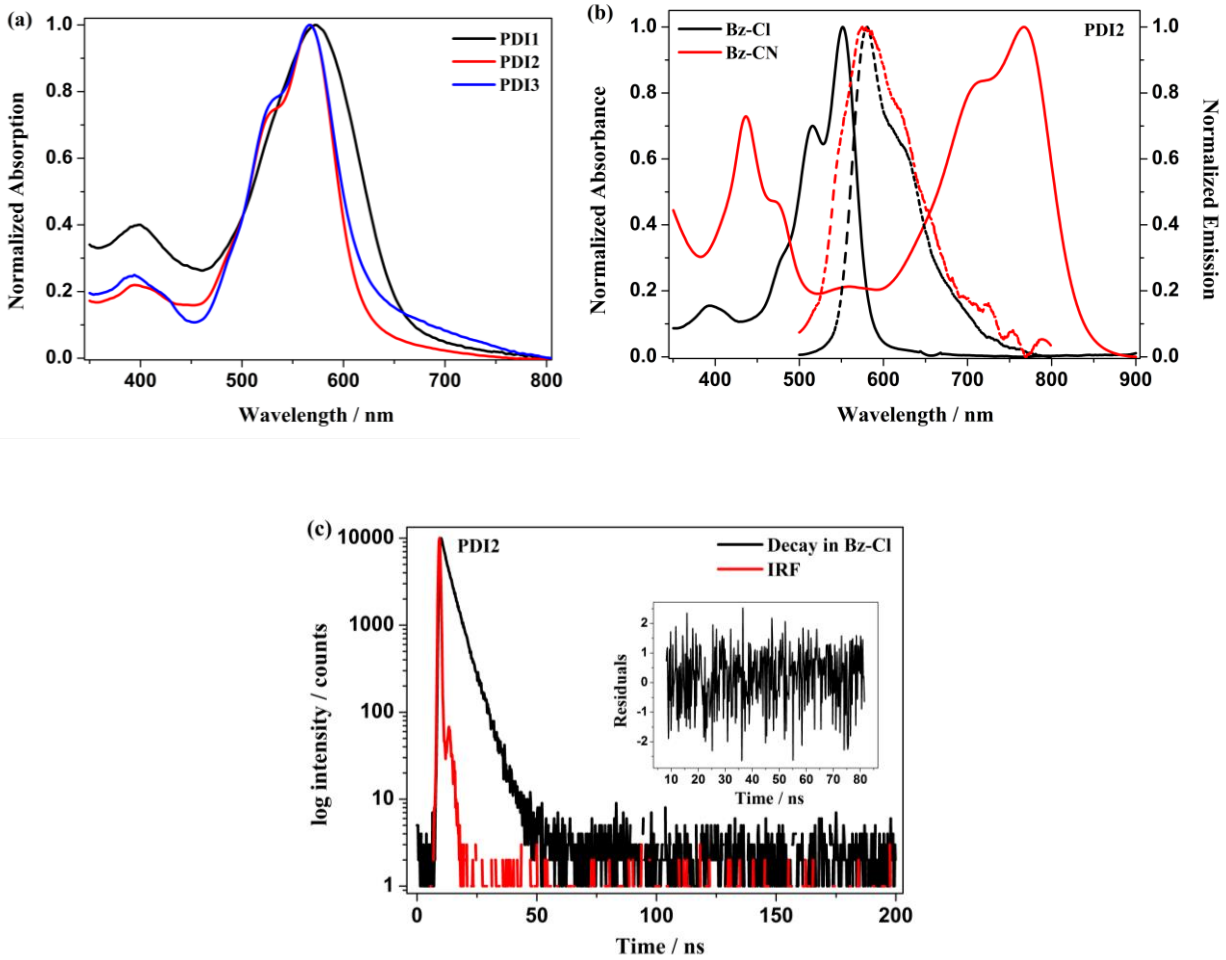


*Fig. 2. (a) Normalized absorption spectra of **PDI1-3** taken on glass substrate. (b) Normalized absorption and emission spectra of **PDI2** dye in chlorobenzene and benzonitrile solutions ($\lambda_{exc}$ = 485 nm). (c) Single photon analysis of **PDI2** dye in chlorobenzene solution. The inset shows the residuals versus time ($\lambda_{detect}$ = 560 nm, $\chi^2$ = 1.04 time increment per channel: 186 ps).*

*Table 1.Fluorescence decay analyses results obtained from the single photon analyses of **PDI2** dye in different solvent of polarities. ($\alpha_i$ (%) indicates the relative amplitudes)[a] ($\lambda_{exc}$ = 485 nm). [a]Relative amplitude values, $\alpha_i$, were calculated with the formula [38]: $W\alpha_i = \tau_i \times P_i / \Sigma\tau_i \times P_i$, where $\tau_i$ was the decay time of the compound, and $P_i$ was the number of free parameters in the fit function ($\lambda_{detect}$ = 560 nm).[b]Fluorescence quantum yields were calculated with reference to fluorescence emission of perylene-3,4,9,10-tetracarboxylic-bis-N,N'-dodecyl diimide ($\Phi_F$ = 1.0 in chloroform, $\lambda_{exc}$ = 485 nm) [39].*

| **PDI2** | $\chi^2$ | $\tau_{f(1)}$ | $\alpha_1$ | $\tau_{f(2)}$ | $\alpha_2$ | $\tau_{f(3)}$ | $\alpha_3$ | $\Phi_F$[b] |
|---|---|---|---|---|---|---|---|---|
| Chloroform | 1.13 | 0.25 | 4.70 | 4.48 | 95.30 | — | — | 0.79 |
| Chlorobenzene | 1.04 | 0.07 | 3.95 | 2.34 | 28.95 | 4.77 | 67.09 | 0.84 |
| Ethanol | 1.13 | 0.38 | 7.57 | 2.92 | 43.36 | 5.69 | 49.07 | 0.19 |
| Benzonitrile | 1.08 | 0.40 | 6.64 | 3.81 | 75.71 | 7.47 | 17.65 | 0.05 |

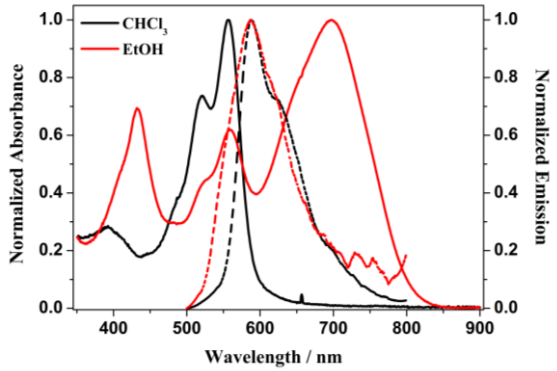


*Fig. S1. Comparison of normalized absorption and emission spectra of **PDI2** dye in chloroform and ethanol solutions ($\lambda_{exc}$ = 485 nm).*

Fig. 3a and Fig. S2a display the UV−vis absorption spectra of **PDI2** and **PDI3** dyes blended with $PC_{71}BM$ (1:2 and 1:3 wt.%), respectively. It can be seen that limited absorption of $PC_{71}BM$ in visible region is enhanced by the addition of PDI dyes incorporating extra band around 570 nm. Adding P3HT to this blend increases the molar absorptivity between 450 and 500 nm (Fig. 3b). Also, when P3HT content of the blend including **PDI1** additive is increased, absorptions at higher wavelengths extend over 700 nm (Fig. S2b).

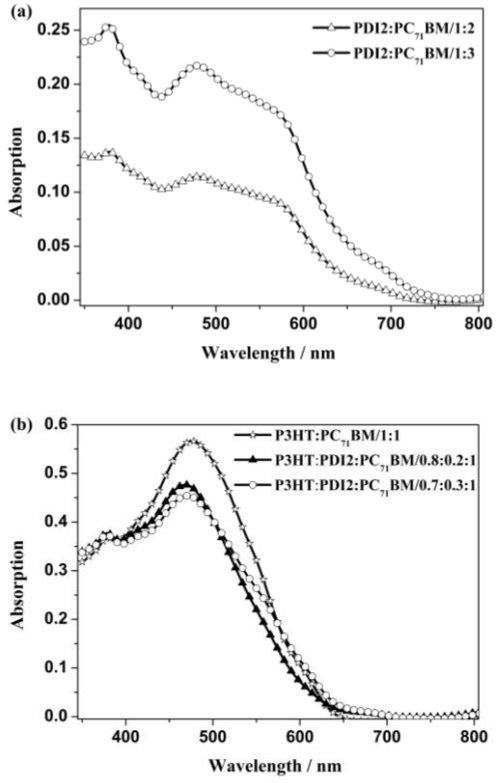


*Fig. 3. (a) Electronic absorption spectra for PDI2:$PC_{71}BM$ (1:2, w/w) and PDI2:$PC_{71}BM$ (1:3, w/w) blend films. (b) Absorption spectra of the blend films of P3HT:$PC_{71}BM$ (1:1, w/w), P3HT:PDI2:$PC_{71}BM$ (0.8:0.2:1, w/w) and P3HT:PDI2:$PC_{71}BM$ (0.7:0.3:1, w/w). All films were grown on substrate without ITO.*

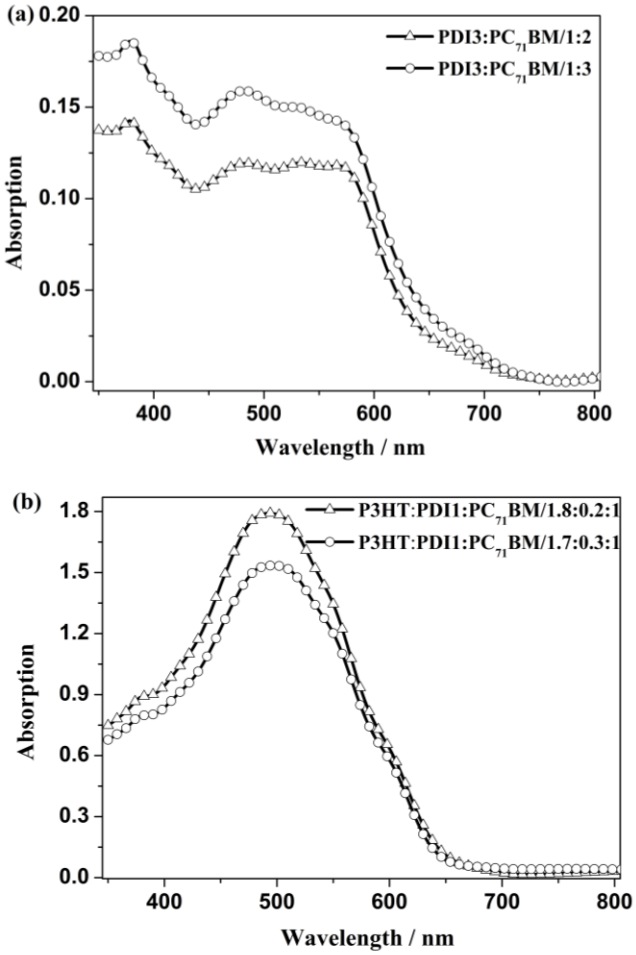


*Fig. S2. Electronic absorption spectra (a) for PDI3:$PC_{71}BM$ (1:2, w/w), PDI3:$PC_{71}BM$ (1:3, w/w), and (b) for P3HT:PDI1:$PC_{71}BM$ (1.8:0.2:1, w/w), P3HT:PDI1:$PC_{71}BM$ (1.7:0.3:1, w/w) blend films. All films were grown on substrate without ITO.*

The fluorescence emissions of PDI dye and $PC_{71}BM$ are centered on 660 and 720 nm, respectively. Fig. 4a and Fig. S3 illustrate the emission spectra of the blend films for two type small molecules of PDI and fullerene. The addition of **PDI2** dye to $PC_{71}BM$ increases the perylene emission and maximum of blend emission spectrum shifts to the blue region slightly. At the same time $PC_{71}BM$ emission in blend films enhances significantly. Enhancement of emission signal for $PC_{71}BM$ is attributed to the fluorescence resonance energy transfer from PDI core to $PC_{71}BM$ small molecule. Similar energy transfer was investigated in detail by Schmidt-Mende et al. [14]. Fig. 4b displays emission spectra for two different mixing ratios of P3HT:PDI2:$PC_{71}BM$ blends at excitation wavelength of 485 nm exciting mainly both P3HT and **PDI2** dye. Enhancement of fullerene emission at 720 nm when adding PDI dye supports the PDI-supported energy transfer from P3HT to $PC_{71}BM$. Similar behavior was observed with higher ratio of P3HT in the blend containing **PDI1** additive (Fig. 4c). When **PDI1** weight ratio is increased from 6.6 to 10% ratio in ternary blend,

marked enhancement of fluorescence emission for $PC_{71}BM$ at wavelength of 720 nm was observed. Small enhancement of PDI weight ratio in the blend is mainly responsible for the increase in $PC_{71}BM$ emission.

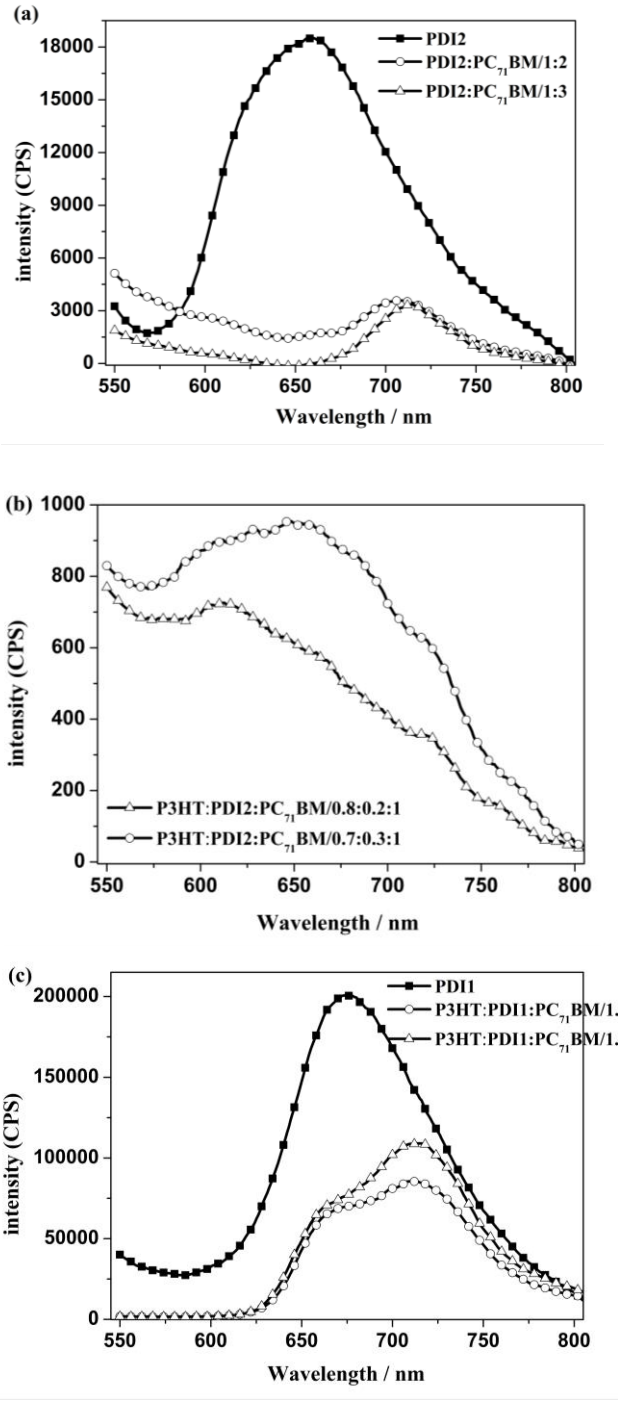


*Fig. 4. Fluorescence emission spectra (a) for pristine **PDI2**, PDI2:$PC_{71}BM$ (1:2, w/w), PDI2:$PC_{71}BM$ (1:3, w/w), and (b) for P3HT:PDI2:$PC_{71}BM$ (0.8:0.2:1, w/w), P3HT:PDI2:$PC_{71}BM$ (0.7:0.3:1, w/w), and (c) for pristine **PDI1**, P3HT:PDI1:$PC_{71}BM$ (1.8:0.2:1, w/w), P3HT:PDI1:$PC_{71}BM$ (1.7:0.3:1, w/w) blend films. All films were excited at 485 nm.*

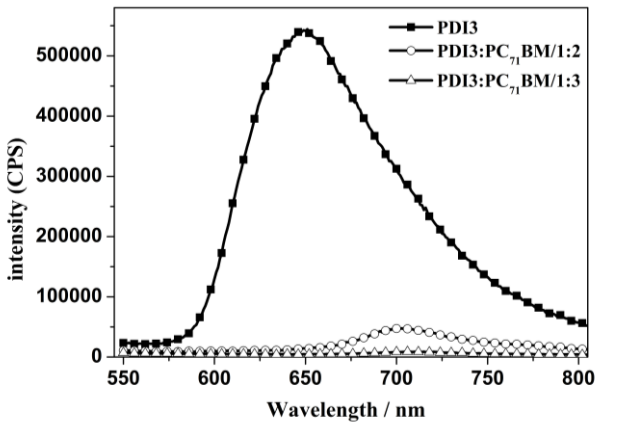


*Fig. S3. Fluorescence emission spectra of pristine **PDI3**, PDI3:$PC_{71}BM$ (1:2, w/w) and PDI3:$PC_{71}BM$ (1:3, w/w) excited at 485 nm.*

The electrochemical properties of **PDI2** dyes have been investigated by using cyclic voltammetry in solution phase. **PDI2** dye gives reduction waves at −0.75 and −1.16 V, indicating the formation of PDI mono and dianion radical, respectively (Fig. S4). The LUMO and HOMO energy levels of **PDI2** dye were calculated to −3.5 and −5.6 eV, respectively. The electrochemcial properties of other studied dyes have been clarified in our previous studies [32, 33]. In addition, HOMO-LUMO energy levels of all used dopants are represented and compared to the energy levels of fullerene and P3HT components in inverted BHJ solar cell configuration in Fig. 5. Energy diagrams for **PDI1-3** dyes in Fig. 5 show that LUMO levels are suitable steps for driving force for an electron transport from P3HT to $PC_{71}BM$. At the same time HOMO levels of the dyes are lower than that of P3HT and higher than that of $PC_{71}BM$, leading to stronger hole injection driving force in ternary BHJ solar cells.

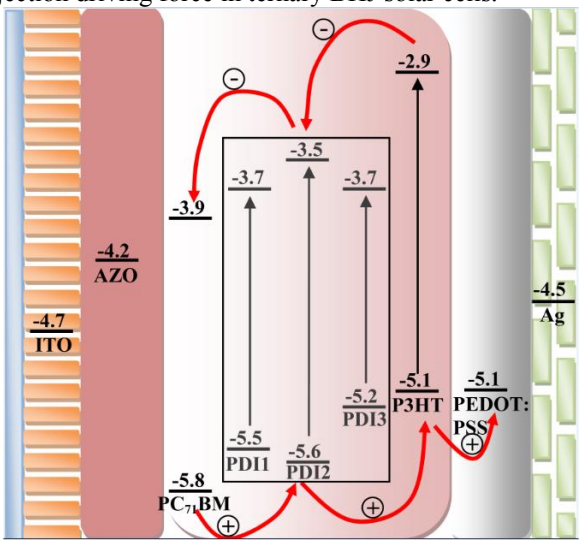


*Fig. 5. Schematic illustration of inverted OPV device structure with experimentally calculated HOMO and LUMO energy band values for PDI type dyes used in this study.*

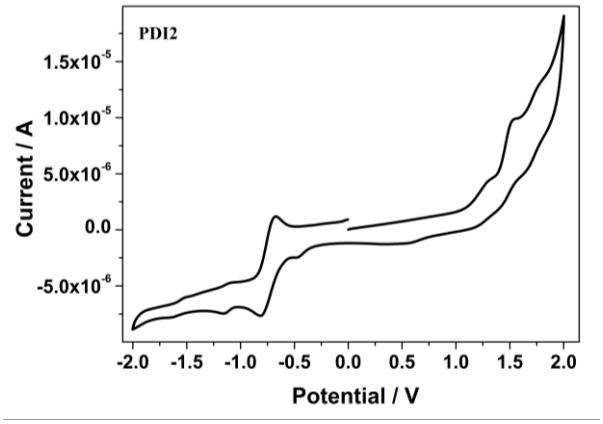


*Fig. S4. Cyclic voltammogram of **PDI2** dye in Me-CN containing [TBA][PF6] at scan rate of 100 mV/s.*

### 3.2 Atomic force microscopy (AFM) images

Active layer morphology brings us valuble data about interpenetrating network in which both the charges are transported to respective electrodes and the photogenerated excitons are separated to get PCE values. Fig. 6a, b and c illustrates the AFM images of thermally annealed films of P3HT:PDI1:$PC_{71}BM$ (1.7:0.3:1, w/w), P3HT:PDI2:$PC_{71}BM$ (0.7:0.3:1, w/w), and P3HT:PDI3:$PC_{71}BM$ (0.7:0.3:1, w/w) blends, respectively. The rms roughnesses of the active layers were 2.46 nm for P3HT:PDI1:$PC_{71}BM$, 2.98 nm for P3HT:PDI2:$PC_{71}BM$ and 2.94 nm for P3HT:PDI3:$PC_{71}BM$, respectively. We have obtained phase separation by doctor-blading on a hot substrate from CB solution, then annealing process at 65 °C. It is known that the coating and annealing process define the crystal dimension of the blend [40, 41]. This medium-size phase separation of PDI-doped ternary films may generate some shunt points resulting in lower PCE. Polycrystalline PDI films posses exciton diffusion ranges of up to 2.5 $\mu$m [42], whereas the exciton diffusion length in conjugated polymers is about 10 nm [24]. Large diffusion length in medium-size phase separation of the films may adversely effect on charge separation at interlayer giving small $J_{sc}$.

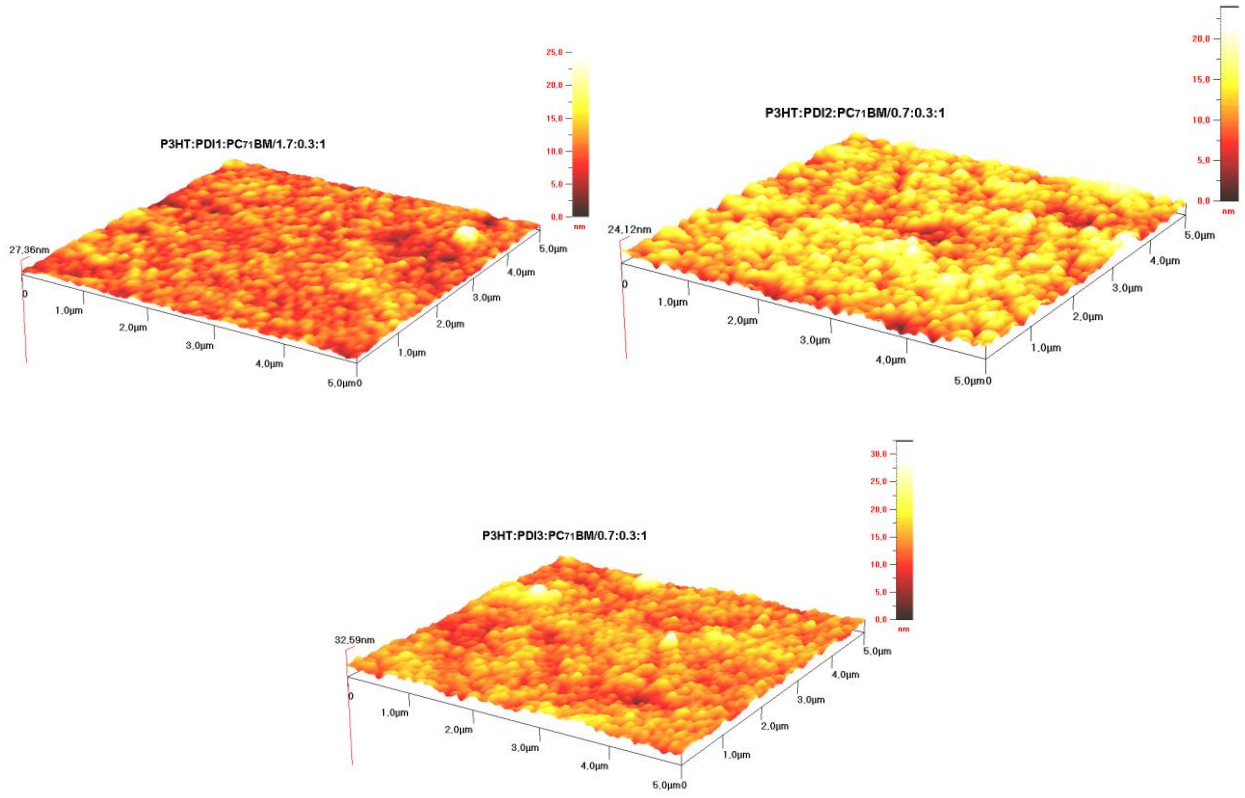


*Fig. 6. AFM images of films with thermally annealed of (a) P3HT:PDI1:$PC_{71}BM$ (1.7:0.3:1, w/w), (b) P3HT:PDI2:$PC_{71}BM$ (0.7:0.3:1, w/w) and (c) P3HT:PDI3:$PC_{71}BM$ (0.7:0.3:1, w/w).*

### 3.3 Device performance and external quantum efficiency (EQE)

Current-voltage characteristics of BHJ solar cells fabricated with non-inverted architecture are shown in Fig. 7a. Devices based on PDI2:$PC_{71}BM$ gives an open-circuit voltage ($V_{oc}$) of 0.62 V, a short-circuit current ($I_{sc}$) of 0.10 mA/cm$^2$, a fill factor (FF) of 24.5%, and a PCE of 0.015% at the best optimized donor/acceptor weight ratio. Also, similar results for **PDI3** dye are summarized in Table 2. These low efficiencies may be explained by the aggregation behavior resulting from the packing of the

molecules [20, 22]. This generates intermolecular recombination points between PDI molecules inhibiting the charge injection. Shin et al. have investigated the effects of functional groups of PDI structures as acceptors in OPV devices and reported that poor morphology of films and aggregating tendency of structures are responsible for low efficiencies [43].

Additionally, the incorporation of **PDI2** dye as an active layer component into inverted BHJ solar cells based on P3HT:$PC_{71}BM$ device has resulted in PCEs of 0.68 and 0.65 for 10 and 15 wt% of the additive dye in ternary blend, respectively. When we introduce **PDI3** as replacement of **PDI2** as shown in Fig. 7b, the $I_{sc}$ of P3HT:PDI3:$PC_{71}BM$ (15 wt% **PDI3** additive) based device has reduced from 3.94 to 1.59 mA/cm$^2$ due to the lower LUMO energy level of **PDI3** with respect to **PDI2** LUMO level. Also, higher HOMO energy level of **PDI3** dye (−5.2 eV) does not supply a significant contribution to the hole transfer process between the $PC_{71}BM$ and P3HT. These are attributed to the rotation of the undecanoxy group out of the perylene ring inhibiting the $\pi-\pi$ stacking interaction of perylene core with P3HT polymer. Both **PDI1** and **PDI2** possesing aromatic rings have higher cell efficiency than that of **PDI3** dye because of suitable fittings of $\pi-\pi$ bonds of aromatic rings with thiophene rings of P3HT polymer. Then, we reduce the PDI dye content and enhance the P3HT weight ratio in the blend to obtain best morphology (Fig. 6a). Compared to the performance of P3HT:$PC_{71}BM$ (2:1 wt%) based device giving 1.05 efficiency, the device using the P3HT:PDI1:$PC_{71}BM$ (1.7:0.3:1 wt%) ternary blend gives higher $I_{sc}$ of 5.33 mA/cm$^2$, higher $V_{oc}$ of 0.60 V and higher FF of 45.2% leading to a PCE of 1.45%. These higher values are attributed to the suitable HOMO-LUMO energy levels and morphology. When we reduce the **PDI1** concentration from 15 to 10 wt% in the blend, PCE value reduces to 1.22%. Although P3HT:PDI1:$PC_{71}BM$ (1.8:0.2:1 wt.%) blend has stronger absorption leading to an increase in light harvesting property in solar spectra than that of P3HT:PDI1:$PC_{71}BM$ (1.7:0.3:1 wt.%) blend (Fig. S2b), a lower PCE value is obtained.

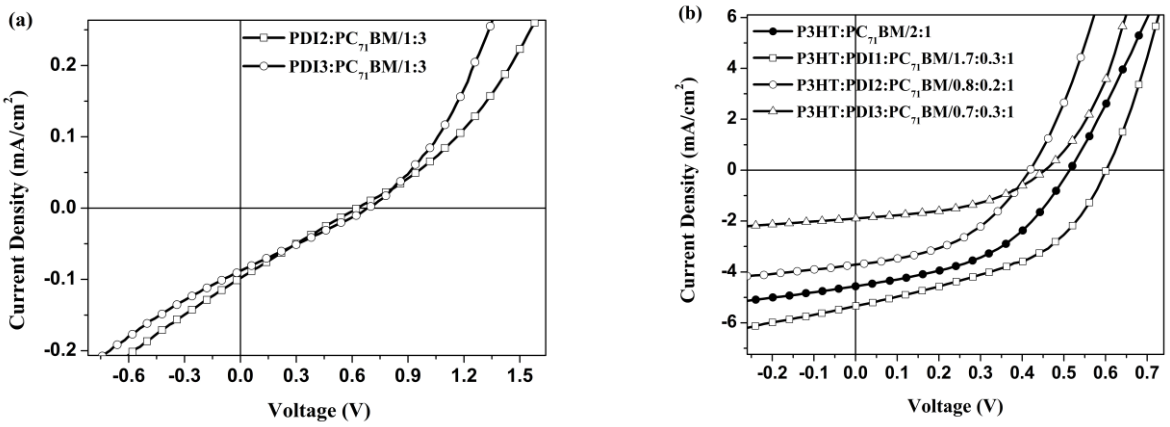


*Fig. 7. Current-voltage characteristics of (a) normal structure of OPVs prepared from **PDI2** and **PDI3** dyes blended with $PC_{71}BM$ as a 1:3 (w/w) ratio and, (b) inverted structure of OPVs made of P3HT/$PC_{71}BM$ and their blended devices with different ratios of **PDI1**, **PDI2** and **PDI3** dyes.*

*Table 2. OPV parameters of normal and inverted structures for BHJ devices prepared from **PDI1-3** dyes.*

| Active Layer | | | | | |
|---|---|---|---|---|---|
| Normal Structure | w:w | $V_{oc}$ (V) | $I_{sc}$ (mA/cm$^2$) | FF (%) | PCE (%) |
| PDI2:$PC_{71}BM$ | 1:3 | 0.62 | 0.10 | 24.5 | 0.015 |
| PDI3:$PC_{71}BM$ | 1:3 | 0.67 | 0.09 | 26.3 | 0.016 |
| Inverted Structure | w:w:w | | | | |
| P3HT:$PC_{71}BM$ | 2:1 | 0.52 | 4.56 | 44.4 | 1.05 |
| P3HT:PDI2:$PC_{71}BM$ | 0.8:0.2:1 | 0.42 | 3.71 | 43.9 | 0.68 |
| | 0.7:0.3:1 | 0.36 | 3.94 | 45.8 | 0.65 |
| P3HT:PDI3:$PC_{71}BM$ | 0.8:0.2:1 | 0.46 | 1.89 | 43.7 | 0.38 |
| | 0.7:0.3:1 | 0.56 | 1.59 | 44.6 | 0.39 |
| P3HT:PDI1:$PC_{71}BM$ | 1.8:0.2:1 | 0.56 | 4.73 | 46.2 | 1.22 |
| | 1.7:0.3:1 | 0.60 | 5.33 | 45.2 | 1.45 |

We measure the EQE of the devices to detect the contribution of PDI additives to photocurrent via absorption. Fig. 8 illustrates the EQEs of all devices giving the best efficiencies. P3HT:PDI1:$PC_{71}BM$ (1.7:0.3:1, w/w) system shows the higher EQE values among the spectra of the blends containing additives, which is consistent with its high $I_{sc}$ at 5.33 mA/cm$^2$ because of its increased EQE values in the regions between 470 and 700 nm. Another striking observation from the EQE spectra is that of the decrease of the EQE signals when adding the PDI dyes resulting the lower PCE values. This observation is attributed to the distortion of $\pi$–$\pi$ bonding arrangement of thiophene polymer initiated by PDI aggregation on polymeric backbone of P3HT, and then reducing the absorption coefficient of the blend. It is understood from EQE, PL measurements and PCE values that the aggregation tendency is higher for **PDI3** dye among the studied other additives in BHJ solar cells. Laquai et al have investigated the aggregation tendency of core- or N-alkylated PDI derivatives in OPV devices and reported that the substitution at PDI aromatic core causes the increased PCE. They have pointed out that substitution at PDI aromatic core has a huge impact on the aggregation in the solid state [23].

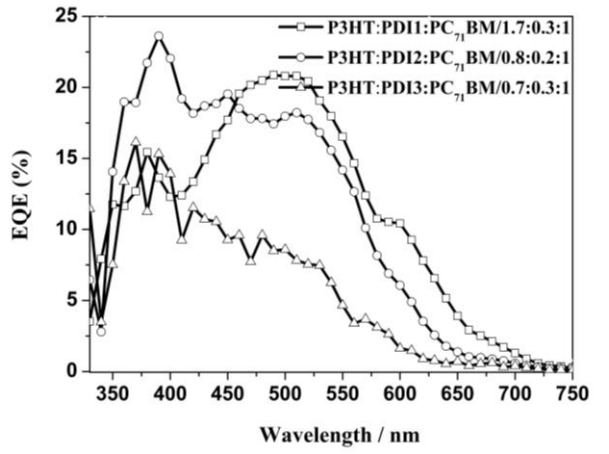


*Fig. 8. EQE spectra for inverted structure of OPV devices blended with different ratios of **PDI1**, **PDI2** and **PDI3** dyes.*

### 3.4 Transport studies

We have used the SCLC measurements to outlook charge mobility for the selected dye of **PDI2** under the conditions for BHJ solar cells as showed in Fig. 9 and Fig S5. In Table 3 charge-carrier mobilities of **PDI2** and **PDI3** dyes are summarized. The hole-only mobilities of PDI2:$PC_{71}BM$ device is obtained as $6.80 \times 10^{-7}$ cm$^2$ V$^{-1}$ s$^{-1}$, whereas that value for PDI3:$PC_{71}BM$ device is about $3.48 \times 10^{-7}$ cm$^2$ V$^{-1}$ s$^{-1}$. These lower data are well correlated with the poor efficiencies at 0.015 and 0.016 for BHJ device fabricated from PDI2:$PC_{71}BM$ and PDI3:$PC_{71}BM$ configurations, respectively. Morever, the electron-only mobilities obtained for P3HT:PDI2:$PC_{71}BM$ (0.8:0.2:1, w/w) device are $1.66 \times 10^{-8}$ cm$^2$ V$^{-1}$ s$^{-1}$. It is understood that **PDI2** dye has a lower contribution to the electron transfer process in ternary blend film as compared to the high electron mobility value around $10^{-3}$-$10^{-4}$ cm$^2$ V$^{-1}$ s$^{-1}$ for P3HT:PCBM blend without any additive materials given in the literature [2].

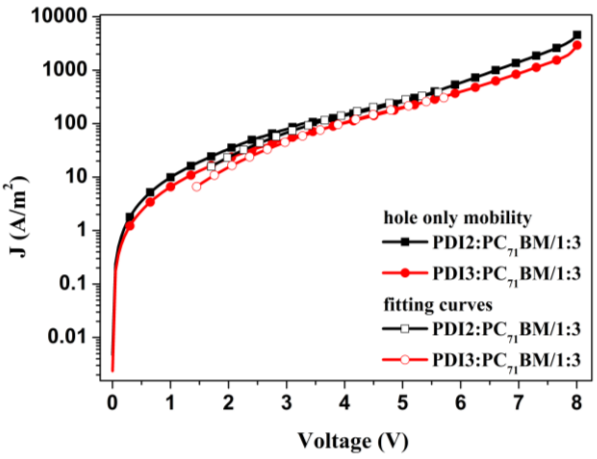


*Fig. 9. Hole only mobility of PDI2:$PC_{71}BM$ (1:3, w/w) and PDI3:$PC_{71}BM$ (1:3, w/w) blend films.*

*Table 3. Hole and electron mobilities of some selected blend films performed by the SCLC measurements.*

| Structure | w:w | $\mu_h$ (cm$^2$ V$^{-1}$ s$^{-1}$) | $\mu_e$ (cm$^2$ V$^{-1}$ s$^{-1}$) |
|---|---|---|---|
| PDI2:$PC_{71}BM$ | 1:3 | $6.80 \times 10^{-7}$ ($R^2$:0.98) | |
| PDI3:$PC_{71}BM$ | 1:3 | $3.48 \times 10^{-7}$ ($R^2$:0.99) | |
| P3HT:PDI2:$PC_{71}BM$ | 0.8:0.2:1 | | $1.66 \times 10^{-8}$ ($R^2$:0.99) |

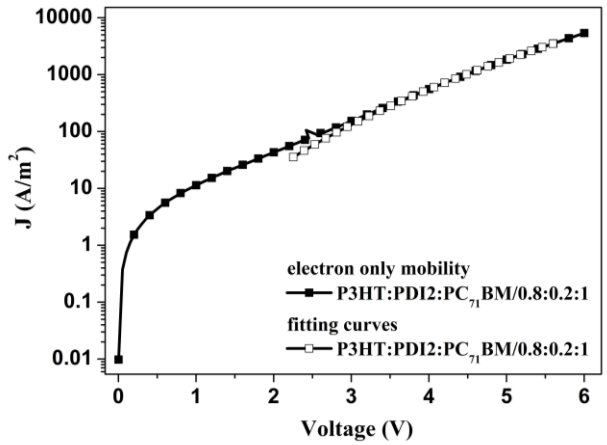


*Fig. S5. Electron only mobility of P3HT:PDI2:$PC_{71}BM$ (0.8:0.2:1, w/w) blend film.*

## 4. Conclusion

In summary, we have investigated the effects of three bay-substituted PDI derivatives on the performance of BHJ solar cells by monitoring the changes in optical absorptions in solution and blend films, morphological properties, energy levels, I-V curves and mobility measurements. Our emission quenching studies show the marked enhancement of fluorescence emission for $PC_{71}BM$ upon addition of PDI derivatives into the blend. These data support the exciton diffusion into the interface of P3HT/PCBM through PDI layer. In addition, aggregation tendency of PDI derivatives (especially for undecanoxy-substituted **PDI3** dye) is mainly responsible for poor cell efficiencies. Thus, by adding 10% weight ratio of **PDI1** additive into the P3HT:PCBM (2:1, w/w) blend film, the cell efficiency was improved by 38% compared to the control cell.

**Acknowledgement**

Financial support for this work was provided by the Research Council of Celal Bayar. University (BAP/2011-056) and the High Education Council of Turkey. The authors would like to thank to Christoph J. Brabec from the institute of materials for electronics and energy technology (I-MEET)-Friedrich Alexander University for giving the opportunity for that use his laboratory in fabricating the photovoltaic devices.

## References

[1] M. Koppe, H.-J. Egelhaaf, G. Dennler, M. C. Scharber, C. J. Brabec, P. Schilinsky, C. N. Hoth, Adv. Funct. Mater. **20**, 338 (2010).
[2] F. Machui, S. Rathgeber, N. Li, T. Ameri, C. J. Brabec, J. Mater. Chem. **22**, 15570 (2012).
[3] Y. Kim, M. Shin, H. Kim, Y. Ha, C.-S. Ha, J. Phys. D: Appl. Phys. **41**, 225101 (2008).
[4] M. A. Ruderer, M. Hinterstocker, P. Müller-Buschbaum, Synth. Met. **161**, 2001 (2011).
[5] J. Chen, X. Yu, K. Hong, J. M. Messman, D. L. Pickel, K. Xiao, M. D. Dadmun, J. W. Mays, A. J. Rondinone, B. G. Sumpter, S. M. Kilbey Ii, J. Mater. Chem. **22**, 13013 (2012).
[6] J. Lee, M. H. Yun, J. Kim, J. Y. Kim, C. Yang, Macromol. Rapid Commun. **33**(2), 140 (2011).
[7] Y.-C. Lai, T. Higashihara, J.-C. Hsu, M. Ueda, W.-C. Chen, Sol. Energy Mater. Sol. Cells **97**, 164 (2012).
[8] D. Qin, W. Quan, J. Liu, G. Li, L. Chen, J. Zhang, D. Yan, Phys. Status Solidi (A) **209**, 1150 (2012).
[9] M. Nam, S. Kim, M. Kang, S.-W. Kim, K.-K. Lee, Org. Electron. **13**, 1546 (2012).
[10] J. P. D. C. Alves, J. N. De Freitas, T. D. Z. Atvars, A. F. Nogueira, Synth. Met. **164**, 69 (2013).
[11] S. Jeong, Y. S. Han, Y. Kwon, M.-S. Choi, G. Cho, K.-S. Kim, Y. Kim, Synth. Met. **160**, 2109 (2010).
[12] S. Jeong, S. H. Woo, H. K. Lyu, C. Kim, H. Kim, Y. S. Han, J. Nanosci. Nanotechol. **12**, 4147 (2012).
[13] Y. Lou, Z. Wang, S. Naka, H. Okada, Appl. Phys. Lett. **99**, 033305 (2011).
[14] H. C. Hesse, J. Weickert, C. Hundschell, X. L. Feng, K. Mullen, B. Nickel, A. J. Mozer, L. Schmidt-Mende, Adv. Energy Mater. **1**, 861 (2011).
[15] D. Rana Bekci, S. Erten-Ela, Renew. Energ. **43**, 378 (2012).
[16] G. Turkmen, H. Sarica, S. Erten-Ela, Solid State Electron. **100**, 61 (2014).
[17] H. Quante, Y. Geerts, K. Mullen, Chem. Mater. **9**, 495 (1997).
[18] X. Zhan, A. Facchetti, S. Barlow, T. J. Marks, M. A. Ratner, M. R. Wasielewski, S. R. Marder, Adv. Mater. **23**, 268 (2011).
[19] H. Dinçalp, S. Içli, Sol. Energy **80**, 332 (2006).
[20] C. Li, H. Wonneberger, Adv. Mater. **24**, 613 (2012).
[21] H. Langhals, J. Karolin, L. B. A. Johansson, J. Chem. Soc.-Faraday Trans. **94**, 2919 (1998).
[22] E. Kozma, M. Catellani, Dyes Pigments **98**, 160 (2013).
[23] V. Kamm, G. Battagliarin, I. A. Howard, W. Pisula, A. Mavrinskiy, C. Li, K. Müllen, F. Laquai, Adv. Energy Mater. **1**, 297 (2011).
[24] X. Guo, L. Bu, Y. Zhao, Z. Xie, Y. Geng, L. Wang, Thin Solid Films **517**, 4654 (2009).
[25] J. R. Knutson, J. M. Beechem, L. Brand, Chem. Phys. Lett. **102**, 501 (1983).
[26] J. Pommerehne, H. Vestweber, W. Guss, R. F. Mahrt, H. Bassler, M. Porsch, J. Daub, Adv. Mater. **7**, 551 (1995).
[27] H. Oh, J. Krantz, I. Litzov, T. Stubhan, L. Pinna, C. J. Brabec, Sol. Energy Mater. Sol. Cells **95**, 2194 (2011).

[28] R. Søndergaard, M. Helgesen, M. Jørgensen, F. C. Krebs, Adv. Energy Mater. **1**, 68 (2011).
[29] N. Li, T. Stubhan, D. Baran, J. Min, H. Wang, T. Ameri, C. J. Brabec, Adv. Energy Mater. **3**, 301 (2013).
[30] T. Stubhan, I. Litzov, N. Li, M. Salinas, M. Steidl, G. Sauer, K. Forberich, G. J. Matt, M. Halik, C. J. Brabec, J. Mater. Chem. **1**, 6004 (2013).
[31] G. D. Sharma, P. Suresh, J. A. Mikroyannidis, M. M. Stylianakis, J. Mater. Chem. **20**, 561 (2010).
[32] H. Dinçalp, Ş. Kızılok, S. İçli, Dyes Pigments **86**, 32 (2010).
[33] H. Dincalp, Z. Askar, C. Zafer, S. Icli, Dyes Pigments **91**, 182 (2011).
[34] T. Kircher, H. G. Lohmannsroben, Phys. Chem. Chem. Phys. **1**, 3987 (1999).
[35] M. Tasior, D. T. Gryko, J. Shen, K. M. Kadish, T. Becherer, H. Langhals, B. Ventura, L. Flamigni, J. Phys. Chem. C **112**, 19699 (2008).
[36] J. Baggerman, D. C. Jagesar, R. a. L. Vallee, J. Hofkens, F. C. De Schryver, F. Schelhase, F. Vogtle, A. M. Brouwer, Chem. Eur. J. **13**, 1291 (2007).
[37] L. Flamigni, B. Ventura, M. Tasior, T. Becherer, H. Langhals, D. T. Gryko, Chem. Eur. J. **14**, 169 (2008).
[38] M. Maus, R. De, M. Lor, T. Weil, S. Mitra, U. M. Wiesler, A. Herrmann, J. Hofkens, T. Vosch, K. Mullen, F. C. De Schryver, J. Am. Chem. Soc. **123**, 7668 (2001).
[39] S. Icli, H. Icil, Spectrosc. Lett. **29**, 1253 (1996).
[40] W. L. Ma, C. Y. Yang, X. Gong, K. Lee, A. J. Heeger, Adv. Funct. Mater. **15**, 1617 (2005).
[41] G. Li, V. Shrotriya, Y. Yao, Y. Yang, J. Appl. Phys. **98**, (2005).
[42] J. J. Dittmer, E. A. Marseglia, R. H. Friend, Adv. Mater. **12**, 1270 (2000).
[43] W. S. Shin, H.-H. Jeong, M.-K. Kim, S.-H. Jin, M.-R. Kim, J.-K. Lee, J. W. Lee, Y.-S. Gal, J. Mater. Chem.**16**, 384 (2006).

*Corresponding author: haluk.dincalp@cbu.edu.tr